Available online at www.sciencedirect.com
ScienceDirect
Journal of Power Sources 177 (2008) 348–354
JOURNAL OF POWER SOURCES
www.elsevier.com/locate/jpowsour

Enhancing liquid water transport by laser perforation of a GDL in a PEM fuel cell

D. Gerteisen *, T. Heilmann, C. Ziegler

Fraunhofer Institute for Solar Energy Systems ISE, Department of Energy Technology, Heidenhofstrasse 2, 79110 Freiburg, Germany

Received 19 September 2007; received in revised form 13 November 2007; accepted 25 November 2007
Available online 4 December 2007

Abstract

The presence of liquid water in a polymer electrolyte membrane fuel cell hinders gas diffusion to the active sites, which results in large concentration overpotentials and instability of the fuel cell performance. In this paper, a new customized gas diffusion layer (GDL) is presented that enhances liquid water transport from the electrode to the gas channels and therefore lowers mass transport losses of oxygen through the porous media. The GDL is systematically modified by laser-perforation with respect to the flow field design. The holes are characterized by SEM images. The performance of the laser-treated GDL was investigated in a small test fuel cell with a reference electrode by voltammetry and chronoamperometry measurements and compared to corresponding data with a non-modified GDL. Voltammetry experiments with different humidification levels of the inlet gases were conducted. In all cases, the cathode overpotential with the perforated GDL clearly shows reduced saturation which can be seen in a lower overpotential in the region limited by mass transport resulting in a higher limiting current density. The investigated current response of the chronoamperometry measurements clearly shows a better dynamic and overall performance of the test cell with the perforated GDL.

Keywords: Proton exchange membrane fuel cell; Liquid water transport; Laser perforation; Gas diffusion layer

1. Introduction

In recent years, the polymer-electrolyte membrane fuel cell (PEMFC) has received great attention as an efficient energy converter. Despite the remarkable progress in PEMFC science and technology during the past decade, optimum water management within the porous components of the PEMFC has not been achieved so far. Droplet and liquid film generation in the channel can be influenced by the contact angle of the channel surface and channel clogging can be managed by appropriate flowfield design and gas purge. The build-up and transport of liquid water in the gas diffusion layer (GDL) depends on the pore size distribution and the contact angle of the pores. Accordingly, the microstructure of GDL materials is a key factor in efficient water management that applies before the water reaches the flowfield. One example of influencing the water management by modification of the porous GDL is the application of a microporous layer (MPL), which reduces the saturation of the GDL at the expense of increased mass transfer resistance. However, the optimization potential within the GDL microstructure is still large with respect to liquid water transport. The pore-flooding phenomenon causes significant loss in cell performance and is problematic for efficient reliable operation under dynamic load conditions and high current density.

Sophisticated measurement techniques for the investigation of liquid water in fuel cells have been developed. Capillary pressure curves, which are one of the most important transport properties of gas diffusion layers, are experimentally determined in [1]. Mercury intrusion porosimetry and the method of standard porosimetry are applied and compared. The role of microporous layers and the hydrophilic porosity are discussed. One way of obtaining a physical visualization of the liquid water transport in GDLs is to apply fluorescence microscopy. Direct observation of the liquid water transport in GDLs was achieved [2]. The results show that the transport in Toray GDLs is a fingering and channeling process. The effect of GDL compression on the water transport behavior was investigated using the same

* Corresponding author. Tel.: +49 761 4588 5205; fax: +49 761 4588 9000.
E-mail address: dietmar.gerteisen@ise.fraunhofer.de (D. Gerteisen).
URL: http://www.ise.fraunhofer.de (D. Gerteisen).

0378-7753/$ – see front matter © 2007 Elsevier B.V. All rights reserved.
doi:10.1016/j.jpowsour.2007.11.080

technique [3]. It is concluded that compression can create preferential hydrophilic channels for water due to the microscopic damage induced to the fiber material and its coating. A number of research groups have developed and applied methods for the in-situ observation of two-phase transport in operating fuel cells. An experimental investigation by X-ray microtomography is presented in [4]. The liquid water saturation in the through-plane direction perpendicular to the direction of the gas channels is measured. The time evolution of the saturation under a purge process is investigated with coarse time resolution. An alternative approach is based on the interaction of neutron radiation and the hydrogen atoms of water. Satija and co-workers [5] used neutron radiography (NR) and tomography for the investigation of liquid water in fuel cells and fuel cell stacks. They also demonstrated methods to quantify the water content of the cell by masking techniques and showed the feasibility of time-resolved neutron imaging. A similar approach based on NR and masking techniques was presented by Kramer and co-workers [6]. An investigation of different flow field types is described, combined with an attempt to quantify the amount of liquid water in the GDL under the ribs. A follow-up paper including fuel cell material variations has since been published [7]. A real-time study of the liquid water build-up in a PEMFC is presented in [8]. Another study applying neutron tomography and high-resolution X-ray imaging was presented in [9,10].

Despite the deep insight into water transport that is provided by the various experimental techniques, the transfer of the results into improved materials has yet to be achieved. In this paper, we develop a method to tailor a common GDL material for improved transport properties with respect to the two-phase flow of air and water. This method is applied to produce a novel GDL prototype that is dynamically tested according to a method proposed in [11] and by chronoamperometry within a test fuel cell.

2. Experimental

We modify a standard Toray paper by producing large pores for the capillary diffusion of liquid water, so that the water can diffuse without requiring large pressure gradients. Simply spoken, we perforate the GDL to obtain water transport channels (WTCs) with a tortuosity of one. Due to the higher in-plane permeability of liquid water compared to the through-plane permeability [12] and the fact that the capillary pressure is lower in larger pores, we assume that the holes "suck" the water from their neighborhood so that the saturation around the hole is reduced. This enhances the oxygen diffusion through the GDL. By providing large pores, the fingering and channeling mechanism as described in [2] is engineered to improve the performance of the cathode. We use a laser beam that cuts out a defined area of the GDL to manufacture the holes. Compared to other possible techniques, the laser technique has the advantage of creating a smoothly cut edge. The carbon fibers are not broken with our technique, so the problem of an inopportunely broken fiber pointing toward the MEA surface, which could cause pin holes, is eliminated. A second advantage of using a laser beam to melt and burn the carbon fibers is the fact that the material is really removed and not just displaced to the surroundings as it would be if needles or similar preparation techniques were used. Displacement of the fibers would lead to rearrangement of the surrounded fibers and definitely to an undesired decrease of the porosity.

2.1. Preparation of the gas diffusion layer

WTCs were cut in the GDL by using a Nd:YAG laser ("Rofin Sinar Laser GmbH") operating at a wavelength of 1064 nm in the near infrared. In the focus of the fixed laser optics, a probe chuck can be moved in the *xy*-plane by a microstepping motor with a position accuracy of 1 μm. A Toray® TGP-H090 was perforated with 39 holes, each of them having a diameter of approximately 80 μm. Fig. 1 (left) shows a SEM image of one hole. It can be seen that the fibers and the binder are really removed, leaving a smooth cut edge. One disadvantage of the laser perforation technique should be mentioned here. If the binder content in the GDL is too high, the binder could melt and cause jamming of the WTC wall. The binder content of the Toray paper used seems to be suitable for our preparation technique. In the assembled cell, the holes are located along the flow channel at a distance of 1 mm to each other so that the liquid water can be removed directly by the gas stream. Fig. 1(right) shows a drawing of the flow field (the rib is colored gray) with the position of the WTCs. The cell size compared to the hole diameter is drawn to scale. The ratio of the area of all circles to the entire GDL surface is

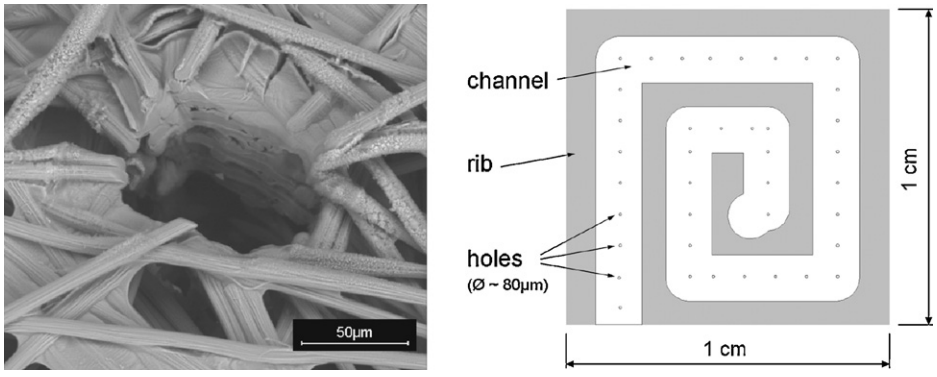

Fig. 1. A hole with a diameter of approximately 80 μm has been burnt into the GDL by a laser beam (left). Schematic drawing of the position and size of the holes along the flow field (right).

only 0.005% and is thus negligible concerning the reduction of the contact area for the electron transport.

2.2. Test cell and operating conditions

The experiments were made with a small test cell in a test bench that are both described in detail in [13] and not repeated here. To investigate the influence of the pore structure of the GDL on the liquid water transport we compare an untreated Toray® TGP-H090 paper with a perforated one (see 2.1). Since the problem of flooding is typically critical on the cathode side only, the cathode GDL is modified by laser treatment, the anode GDL remains untreated in all experiments. A Gore™PRIMEA® Series 5510 membrane electrode assembly (loading$_{c/a}$: 0.4/0.4 mg cm^{-2}, thickness: 35 μm) was used in both cases. Polarization curves were measured in potentiostatic mode with a scan rate of 10 mV s^{-1} in the range of 900–60 mV. During the experiment the cell impedance (10 kHz), cathode overpotential, anode overpotential and cell temperature were recorded. The air flow rate was set to 100 ml min^{-1} on the cathode side and the hydrogen flow rate was set to 50 ml min^{-1} on the anode side. Depending on the experiment, humidified or dry gases were used and are specified directly in the result section for each polarization curve. The fuel cell was cooled by a water cooling circuit with a thermostat ($T_{\text{thermostat}} = 40\,^{\circ}\text{C}$) to maintain the temperature of the cell in a defined range. Nevertheless, the cell heated up at high current densities due to ohmic heating, so the cell temperature fluctuated over a range of $\Delta T \approx 4\,^{\circ}$ C during a voltammetry cycle. Several cycles in succession were operated to ensure repeatability and to approximate dynamic equilibrium.

With the same operating conditions, chronoamperometry is used as a second characterization technique with a new assembled cell. The current response and cell impedance induced by voltage steps from 0.8 to 0.5 V, 0.7 to 0.4 V, 0.6 to 0.3 V and backwards are analyzed. A higher coolant flow rate than for the voltammetry experiments was chosen to maintain a comparable temperature evolution between the measurements with and without perforated GDLs

3. Results

By using a normal hydrogen reference electrode (NHE) in the test fuel cell, the voltage loss under load has been separated into cathode overpotential, anode overpotential and ohmic overpotential as follows:

- The ohmic overpotential is calculated by Ohm's law with the measured current density (i_{cell}) and the measured cell impedance ($Z_{10\text{kHz}}$)

$$\eta_{\Omega} = i_{\text{cell}} Z_{10\text{kHz}}, \tag{1}$$

where

$$Z_{10\text{kHz}} = Z_{\text{mem}} + Z_{\text{contact}} \tag{2}$$

is the sum of the membrane resistance (Z_{mem}) and the contact resistances (Z_{contact}). The electronic losses in the bulk material (current collector, GDL, electrode) are negligible.

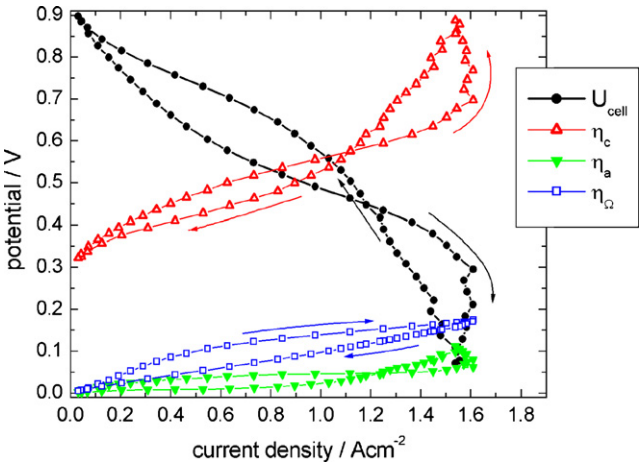

Fig. 2. A typical voltammetry measurement that shows MEA dehydration at high cell voltage and flooding in the limiting current-density region which results in two hysteresis loop like a "eight". The loss mechanisms are separated into cathode, anode and ohmic overpotential.

- The anode overpotential is defined as the potential difference between the anode current collector (AC) and the NHE, corrected by the ohmic drop between AC and NHE [13]. This ohmic drop has been taken into account by the assumption of a symmetric potential distribution in the membrane and equal contact resistances on the cathode and anode side, which leads to an overpotential correction of the half cell impedance multiplied by the current density

$$\eta_a = \Phi_{\text{AC}} - \Phi_{\text{NHE}} - \frac{1}{2} i_{\text{cell}} Z_{10\text{kHz}}, \tag{3}$$

- The cathode overpotential is defined as the difference between the cathode current collector (CC) and the NHE with respect to the theoretical open circuit voltage of 1.23 V. The data are corrected by the ohmic drop between CC and NHE, in making the same assumptions as for the anode overpotential correction

$$\eta_c = 1.23 - (\Phi_{\text{CC}} - \Phi_{\text{NHE}}) - \frac{1}{2} i_{\text{cell}} Z_{10\text{kHz}}. \tag{4}$$

Fig. 2 shows in advance of the following discussion a representative example of one IU-curve and the separated overpotentials of the present experimental study. The cell was operated in potentiostatic mode from 900 to 60 mV (forward mode) and back to 900 mV (backward mode) with dry gas streams (case (1)). The cell voltage shows a strong hysteresis between the forward and backward sweeps. Beginning with a relatively dry membrane electrode assembly (MEA) at 900 mV the cell voltage decreases fast with increasing load. A steep decline at a current density of 1.6 A cm^{-2} indicates flooding of the porous media, despite the dry inlet streams. In the backward mode, the cell voltage suffers from the flooding event up to a current density of approximately 1.2 A cm^{-2}, where the IU-curve in the backward mode crosses the one in forward mode. From then on, the higher humidification of the porous media and MEA leads to better performance in the backward mode.

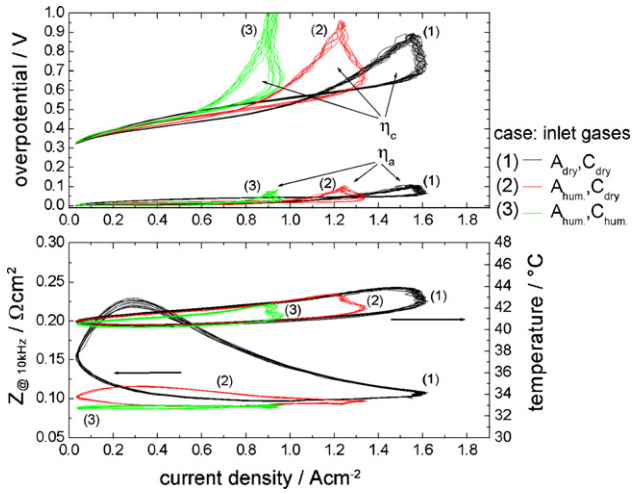

Fig. 3. Cathode and anode overpotentials of voltammetry measurements with an original Toray® paper. The influence of the feed streams was investigated: case (1) with dry feed streams, case (2) with the anode feed stream humidified, case (3) with both feed streams humidified (top). The increase of the cell impedance for low current-density indicates dehydration of the membrane. The temperature fluctuates between 40.5 and 44 ° C during a cycle (bottom).

It can be seen that the cathode overpotential η_c (Eq. (4)) is responsible for the rapid drop at high current-density when flooding occurs. The main part of the hysteresis in the low current-density region can be attributed to the ohmic loss η_Ω (Eq. (1)) that clearly highlights the effect of hydration/dehydration. This large difference of the ohmic overpotential between the forward and backward modes is responsible for the change in the activation overpotential at the electrodes for a given cell voltage.

3.1. Voltammetry experiment

Figs. 3 and 4 show the behavior of the cathode and anode overpotential during voltammetry measurements of 10 cycles.

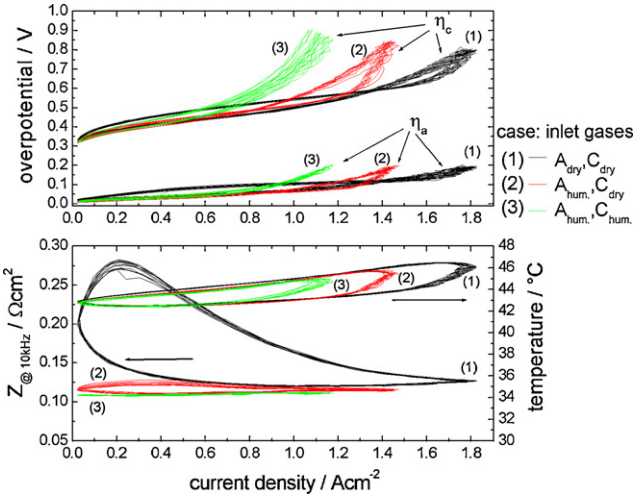

Fig. 4. The measurements with the perforated cathode GDL shows reduced flooding and thus higher limiting current densities (top). Due to a slightly higher cell impedance and higher currents, the temperature increased to 42.5–46.5 ° C (bottom).

Repeatability and dynamic equilibrium are assured. Three different operating conditions were chosen for the experiments:

(1) Dry inlet gas streams on the cathode and anode side,
(2) Dry air and humidified hydrogen ($T^{H_2}_{\text{dew point}} = 37\,^\circ\text{C}$),
(3) Humidified air ($T^{\text{air}}_{\text{dew point}} = 37\,^\circ\text{C}$) and humidified hydrogen ($T^{H_2}_{\text{dew point}} = 37\,^\circ\text{C}$).

In all three cases, Fig. 3(top) indicates flooding when the limiting current-density (i_{lim}) is reached, as characterized by the hysteresis shoulder in the high current-density region. The measurement with two dry inlet feed streams shows the highest current density ($i_{\text{lim}} = 1.6\,\text{A}\,\text{cm}^{-2}$) which obviously indicates that flood starts later than in case (2) and (3). While the porous media is flooding, the current density is decreasing with increasing overpotential due to accumulation of water over time in all three cases. The high limiting current density of case (1) is paid by a strong dehydration of the MEA in the low current-density region, which is indicated by the increasing cell impedance (Fig. 3 bottom). In case (2), weak dehydration of the MEA can also be observed whereas in the case of both gas streams being humidified (3), the impedance remains nearly stable at a value of approximately 88 m $\Omega\,\text{cm}^2$. The anode losses η_a (Eq. (3)) are small but not negligible in all cases and reach a maximum value of 100 mV at i_{lim}. The heat of reaction and the ohmic losses are responsible for the heating of the cell by up to 3.5 ° C during a cycle.

Fig. 4 shows the same experiments as Fig. 3 but with a perforated cathode GDL. The characteristic of the polarization curve in the high current-density region has clearly changed. The hysteresis loop due to flooding was minimized. The sudden increase of the cathode overpotential in the limiting current-density region was reduced, so i_{lim} was reached with the highest overpotential. In all three cases, a boost to higher i_{lim} of 8–22% has been achieved. In these measurements, the cell impedance was significantly higher with the perforated GDL. It was not possible to reduce the impedance to a level of 88 m $\Omega\,\text{cm}^2$ as in the first experiment (Fig. 3), not even with fully humidified gas streams. Thus, we assume that this impedance shift results from a slightly higher contact resistance. The increased performance loss at the anode (approximately 200 mV at i_{lim}) could be an indication for a poor contact on the anode side. Due to this higher basic impedance and the higher current density, the cell heats up to a temperature 2 ° C above the temperature of the first experiment. This fact in turn leads to stronger dehydration of the MEA in the low current-density region in the case of dry reactant gases (1), as validated by the increase of the cell impedance.

In Fig. 5, a direct comparison of UI-curves (left) and cathode polarization curves (right) is made between the operation with the original and the perforated GDL. For clarity, only the cases (1) and (3) are depicted in the graph. On the left-hand side, the IU-curves with the perforated GDL show a higher limiting current density, as discussed before, but rather a small decline than an improvement of the cell voltage at a given current density is observed. This fact is caused by the above mentioned higher basic impedance and the resulting higher anode losses, lower-

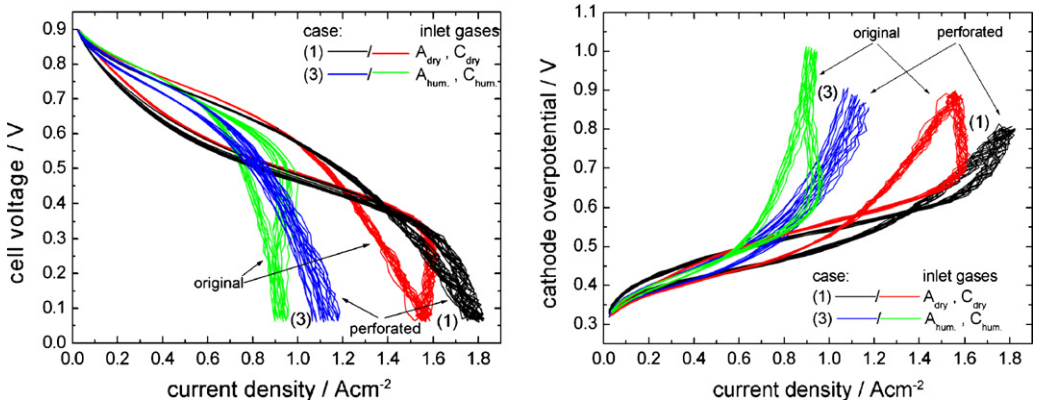

Fig. 5. A comparison between the non-modified and perforated GDL clearly shows a reduced mass transport limitation due to reduced saturation of the porous media in the high current-density region. The higher basic impedance of the fuel cell with the perforated GDL and the resulting increased temperature prevents a better performance at low current densities due to dehydration (left). A reduced saturation level of the perforated GDL can be supposed by the characteristic of the separated cathode overpotential (right).

ing the cell voltage. For analyzing the enhancement of the liquid water transport we refer to the cathode losses depicted on the right-hand side of Fig. 5. In the low current-density region, the polarization curves with the original and perforated GDL are identical. Turning to high current densities, the cathode polarization curves with the unmodified GDL start to suffer from transport limitations earlier and finally show a sudden increase of the overpotential. It is obvious that this increase of the overpotential is missing in the polarization curve with the perforated GDL, indicating a reduced pore flooding.

3.2. Chronoamperometry

Investigations concerning the transient behavior of the current response on voltage step changes and the corresponding impedance response are shown in Figs. 6–8 . The cell was operated with dry air and humidified hydrogen ($T^{H_2}_{\text{dew point}} = 39\,^{\circ}\text{C}$). Gas flow rates and coolant temperature are equal to the voltammetry experiments. In Fig. 6 the cell voltage was stepped between 0.8 and 0.5 V. The current response is shown on the left-hand side. An overshoot is depicted in both cases whereas the peak current density is approximately $0.2\,\text{A}\,\text{cm}^{-2}$ higher with the perforated GDL and ends $0.1\,\text{A}\,\text{cm}^{-2}$ above the original GDL. A higher current density is also observed at 0.8 V. A strong dehydration can be reasoned from the impedance data at 0.8 V, pictured in Fig. 6(right). The water generation by the ORR seems not to be sufficient to prevent dehydration of the iosomer, whereas the dehydration is more pronounced with the original GDL due to the lower current density. The cell impedance drops very fast when applying a cell voltage of 0.5 V. Fig. 7 shows the dynamics of the current density and the impedance on a step change from 0.7 to 0.4 V and backwards. The peak current densities are similar to each other but the decline with the laser-treated GDL is less strong, resulting in an improvement of the

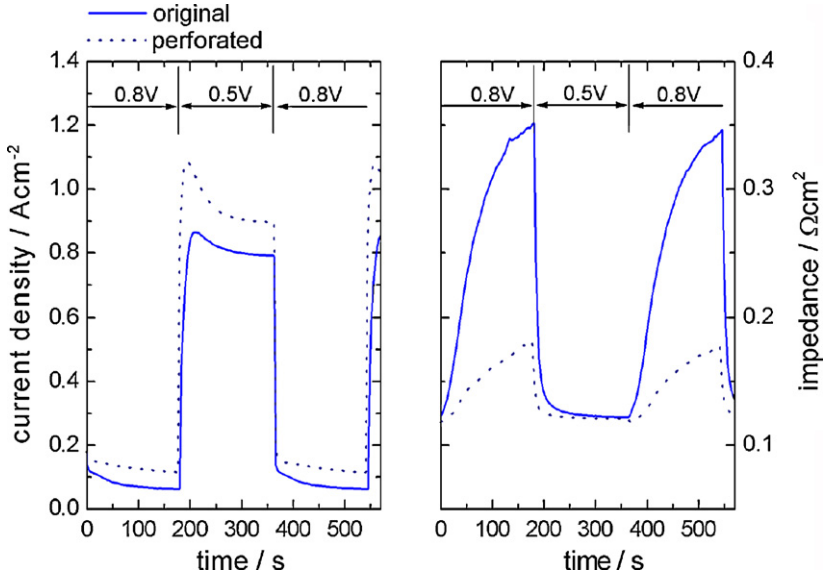

Fig. 6. The test cell with perforated GDL shows a significantly higher current density than the cell with the original GDL (left). The cell impedance shows that water generation by the ORR is not sufficient to prevent dehydration of the iosomer at a cell voltage of 0.8 V (right).

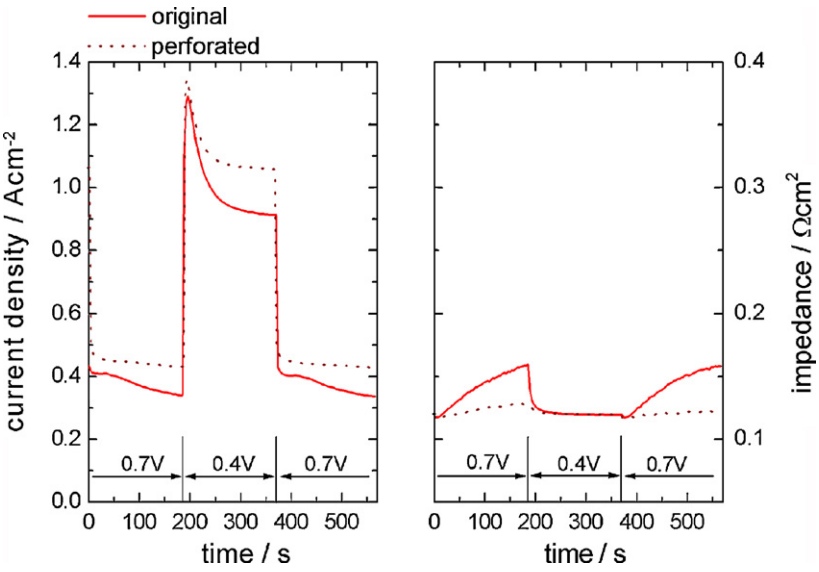

Fig. 7. The current density response with the original GDL show a strong decay of the peak current due to pore flooding (left). The current density range between 0.3 and 0.5 A cm^{-2} seems to be a critical value for a stable humidification of the membrane (right).

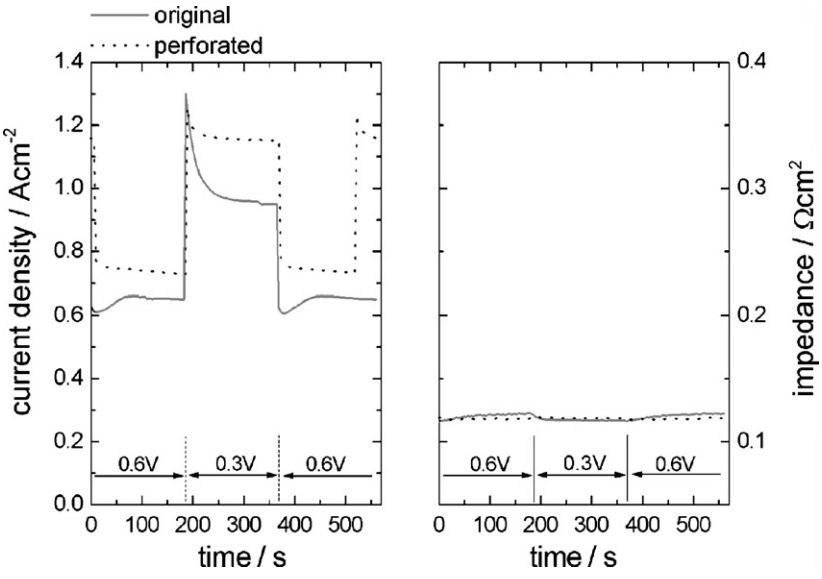

Fig. 8. A pronounced overshoot and undershoot behavior is observed in the current response for the cell with original GDL, whereas only a small overshoot is recorded with the perforated GDL. This clearly indicates a lower saturation level for the latter (left). The impedances are identical and stable over time (right).

power density of about 15%. Due to the higher current density with the perforated GDL at a voltage of 0.7 V, the water generation is large enough to maintain a stable impedance. By contrast, the dehydration in case of the original GDL leads to a decrease in the current density several seconds after the voltage change. The voltage change from 0.6 to 0.3 V and backwards is investigated in Fig. 8. Only a small overshoot is recorded in case of the perforated GDL that results in an improvement of the power density of about 20%. An undershoot behavior is observed in case of the original GDL, stepping from 0.3 to 0.6 V. This phenomenon can be explained by a reduction of the saturation level when switching to lower current densites, this in turn leads to a performance improvement over time, until a new equilibrated saturation is reached. Both impedances remain stable at the same value, shown in Fig. 8(right).

4. Conclusion and outlook

A customized GDL, structured with water transport channels by laser perforation, was prepared and investigated in a test fuel cell with an active area of 1 cm^2. The laser-cut holes with a diameter of approximately 1 μm are spaced along the channel at a distance of 1 mm. A comparison with a standard, non-modified GDL shows that the performance with the perforated GDL suffers less from accumulated liquid water. The cathode overpotential shows less limitation of the oxygen transport. An increase in the limiting current density of 8–22% with the perforated GDL has been achieved. A comparison of chronoamperometry data shows clearly reduced overshoot behavior, ending in a higher current density value in case of the perforated GDL. This highlights the achievement of less pore flooding and an enhanced

water transport in the GDL. The potential to optimize the GDL structure with regard to liquid water transport, resulting in a reduced water accumulation and minimized oxygen diffusion limitation, is still very large.

This systematic perforation technique can play an important role in the transition to large fuel cells and stacks, where engineers have to cope with strong in-plane inhomogeneities in humidification, saturation and temperature from inlet to outlet. With respect to the flow field geometry and operating conditions, a tailor-made GDL can be manufactured by the laser perforation technique to compensate for these inhomogeneities by specific arrangement and diameters of the water transport channels.

Another application of the presented perforation technique is for direct methanol fuel cells. Systematic positioning of holes in the GDL can help to remove the CO_2 bubbles that are by-products of the methanol oxidation and therefore to achieve more stable performance, especially in passive systems.

References

[1] J. Gostick, M. Fowler, M. Ioannidis, M. Pritzker, Y. Volfkovitch, A. Sakars, J. Power Sources 156 (2) (2006) 375–387.
[2] S. Litster, D. Sinton, N. Djilali, J. Power Sources 154 (2006) 95–105.
[3] A. Bazylak, D. Sinton, Z.-S. Liu, N. Djilali, J. Power Sources 163 (2007) 784–792.
[4] J. Kowal, A. Turhan, K. Heller, J. Brenzier, M. Mench, J. Electrochem. Soc. 153 (10) (2006) A1971–A1978.
[5] R. Satija, D. Jacobson, M. Arif, S. Werner, J. Power Sources 129 (2004) 238–245.
[6] D. Kramer, J. Zhang, R. Shimoi, E. Lehmann, A. Wokaun, K. Shinohara, G. Scherer, Electrochim. Acta 50 (2005) 2603–2614.
[7] J. Zhang, D. Kramer, R. Shimoi, Y. Ono, E. Lehmann, A. Wokauna, K. Shinora, G. Scherer, Electrochim. Acta 51 (2006) 2715–2727.
[8] M. Hickner, N. Siegel, K. Chen, D. McBrayer, D. Hussey, D. Jacobson, M. Arif, J. Electrochem. Soc. 153 (5) (2006) A902–A908.
[9] I. Manke, C. Hartnig, M. Gruenerbel, W. Lehnert, N. Kardjilov, A. Haibel, A. Hilger, J. Banhart, H. Riesemeier, Appl. Phys. Lett. 90 (2007) 174105.
[10] I. Manke, C. Hartnig, M. Gruenerbel, W. Lehnert, N. Kardjilov, A. Haibel, A. Hilger, J. Banhart, W. Treimer, M. Strobl, Appl. Phys. Lett. 90 (2007) 184101.
[11] C. Ziegler, H. Yu, J. Schumacher, J. Electrochem. Soc. 152 (2005) A1555–A1567.
[12] V. Schulz, J. Becker, A. Wiegmann, P. Mukherjee, C.-Y. Wang, J. Electrochem. Soc. 154 (2007) B419–B426.
[13] D. Gerteisen, J. Appl. Electrochem. 37 (2007) 1447–1454.